Lab on a Chip

PAPER

View Article Online
View Journal | View Issue

Cite this: *Lab Chip*, 2023, **23**, 3694

Simple modification to allow high-efficiency and high-resolution multi-material 3D-printing fabrication of microfluidic devices†

Reverson Fernandes Quero,[a]
Dosil Pereira de Jesus [ab] and José Alberto Fracassi da Silva *[ab]

Received 24th April 2023,
Accepted 7th July 2023

DOI: 10.1039/d3lc00356f

rsc.li/loc

Advances in the instrumentation and materials for photopolymerization 3D printing aided the use of this powerful technique in the fabrication of microfluidic devices. The costs of printers and supplies have been reduced to the point where this technique becomes attractive for prototyping microfluidic systems with good resolution. With all the development of multi-material 3D printers, most of the microfluidic devices prepared by photopolymerization 3D printing are based on a single substrate material. We developed a digital light processing multi-material 3D printer where two or more resins can be used to prepare complex objects and functional microfluidic devices. The printer is based on a vat inclination system and embedded peristaltic pumps that allow the injection and removal of resins and cleaning step between material changes. Although we have built the whole system, the modification can be incorporated into commercially available printers. Using a high-resolution projector, microfluidic channels as narrow as 43 μm were obtained. We demonstrate the printing of multi-material objects containing flexible, rigid, water-soluble, fluorescent, phosphorescent, and conductive (containing PEDOT or copper nanoparticles) resins. An example of a microfluidic chip containing electrodes for electrochemical detection is also presented.

1. Introduction

Microfluidics is the field of science that deals with the transport of fluids in confined channels with dimensions of tens to a few hundreds of micrometers.[1] Introduced by Manz *et al.* in the early 90s, micro total analysis systems (μTAS)[2] (or simply 'microchips') conceptualize the integration of several analytical steps into a single substrate to perform complete analytical procedures, which can include fluid motion control (pumping), sample treatment, sorting (or separation), and detection.[3] Initially, the microchip microfabrication took advantage of the protocols used in the microelectronic industry and was based on photolithography, which has high associated costs. The introduction of PDMS-based processes by Duffy *et al.*[4] accelerated the development of microfluidic devices, but in general, soft lithography is a 2D fabrication technique, which makes it difficult to obtain devices with complex geometry.[5]

In the context of the fabrication of microfluidic devices, additive manufacturing (or 3D printing) is very promising, as it enables the generation of objects with high structural complexity. In this way, the integration of connectors and cavities for coupling different parts (for example, tubes, optical fibers, and electrodes) is natural and can be incorporated into the manufacturing process. As expected, the use of 3D printing has accelerated in recent years due to improvements in printers, development of new materials, and introduction of new printing methodologies. Many groups have demonstrated the capabilities of 3D printing for the production of microfluidic devices,[6–24] including the comparison of different printing techniques.[25,26] The use of 3D printing in microfluidics has also been reviewed.[1,26–31]

Although microfluidic devices can be successfully created in a single material substrate, the use of multi-material printing allows the addition of features to the devices, promoting more functionality to them. Complete lab-on-a-chip devices could be one-step printed in order to incorporate conductive tracks for electric field application and electrochemical sensing, porous materials for filtration, preconcentration and separation, flexible membranes for valve actuation and pumping, among other applications. Fused deposition modeling (FDM) is a straightforward way to implement devices containing multi-materials[32–34] since two or more extruders can be combined to deposit different

[a] *Institute of Chemistry, State University of Campinas, Campinas, SP, 13083-861, Brazil. E-mail: fracassi@unicamp.br*
[b] *Instituto Nacional de Ciência e Tecnologia em Bioanalítica (INCTBio), Campinas, SP, Brazil*

† Electronic supplementary information (ESI) available. See DOI: https://doi.org/10.1039/d3lc00356f

materials. Print pausing has been used to introduce parts during the printing process,[35] but this method cannot be named a truly multi-material printing. In spite of the fact that some progress has been made to improve the resolution of FDM 3D printing,[12,24,36] it is still challenging to produce devices containing channels with dimensions below 100 μm. Inkjet[37] and direct ink writing[38] are also prone to multi-material deposition, but due to the vertical direction of deposition and the fluidity of the inks, a sacrificial material is necessary to create embedded channels and chambers. This fact itself is not a problem, but the removal of these sacrificial layers in the microscale can be troublesome, leading to clogged microchannels.[25] Additionally, the resolution of these techniques is the limit to produce channels with dimensions below 100 μm, and the roughness of the microchannels is impaired by the removal of the sacrificial layer. Conversely, digital light processing (DLP) offers a suitable resolution level to produce microfluidic devices, as demonstrated by the research groups of Woolley and Nordin from Brigham Young University,[15–21] where the production of microchannels as narrow as 20 μm was demonstrated.[20]

Advances in instrumentation have allowed multi-material printing in DLP. Recently, Shaukat *et al.* have published a comprehensive review on this topic.[39] According to the authors, there are three main strategies for multi-material vat photopolymerization: (1) by changing resins in one or more vats, (2) by changing the light source to promote orthogonal photopolymerization reactions, and (3) by varying the light intensity. In the context of this work, it is important to describe the first strategy of multi-material vat photopolymerization 3D printing. According to Shaukat *et al.*,[39] the first to describe multi-material stereolithography 3D printing was Maruo *et al.* in 2001.[40] In 2004 and 2006, the research group of Ryan Wicker presented an automated multi-material stereolithography printer based on a rotating four-vat carousel,[41,42] following publications in 2010 (ref. 43 and 44) and 2011 (ref. 45) and a review in 2012.[46] The potential to incorporate conductive tracks and electronic parts into printed devices was also demonstrated in 2012 and 2014.[47,48] The years that followed saw refinements to these basic ideas and examples of multi-material 3D printing applications. Ge *et al.* used the vat exchanging strategy to 3D print different tailored shape memory polymers (4D printing).[49] Instead of using a "physical" vat, Wang *et al.* deposited resins over a delivery wheel mounted on a stepper motor.[50] In 2018, Kowsari *et al.* used a similar approach by placing the resins in a linear stage made in borosilicate glass covered by a polytetrafluoroethylene film.[51] In their approach, a high resolution was achieved (15 μm pixel size) by using a high-contrast digital microdisplay. Also, an air jet was delivered to the substrate after layer exposure for the removal of resin residues. Subsequently, Kowsari *et al.* studied the influence of the resin monomers on the quality of the printed objects. Outstanding roughness and transparency were achieved by using 1,6-hexanediol dimethacrylate (HDDMA).[52] Other applications from this research group involve the production of multi-material 3D-printed stretchable hydrogels[53] and pneumatic actuators for soft robots.[54] In 2018, Kim *et al.* described the integration of porous membranes in a microfluidic chip by manually pausing a commercial printer at the desired layer and changing the resin vat.[55] Changing vats was also the strategy employed by Khatri *et al.*,[56] but in this case, the authors built their low-cost automated printer. In a different approach, Mao *et al.* developed an instrument containing printing heads to allow "coating, curing, cleaning, and post-curing" (C3P).[57] Ahmed *et al.* pointed out that the time spent for the fabrication of a microfluidic chip was decreased from 6 to 2 h by applying a protocol of multi-material 3D printing when compared to the conventional 3D mold printing and polydimethylsiloxane replication.[58] The authors used multi-material approach to combine flexible and rigid materials to integrate pneumatic valves into the microfluidic chips in a one-step process. Lipkowitz *et al.* introduced a modification of the Continuous Liquid Interface Production (CLIP) to allow the injection of the photo-resin in a process the authors called injection continuous liquid interface production (iCLIP).[59] The injection of resin increased the printing velocity and also allowed the preparation of multi-material objects. Mayer *et al.*[60] used 3D direct laser writing (DLW) with two-photon polymerization (2PP) and a microfluidic chamber to print 3D fluorescent-layered structures. The use of a flow controller and a multiport valve allowed the selection of up to seven liquids with an injection volume of about 0.5 mL. The 2PP processes guaranteed an outstanding resolution at the cost of small print volume. In a similar approach, Lamont *et al.* used 2PP-DLW to prepare a template for PDMS mold replication.[61] Multi-material 3D printing was then conducted inside the PDMS microchannel.

From the previous examples, it is clear that multi-material DLP 3D printing is a powerful tool for the preparation of functional microfluidic devices. In this work, we describe an alternative approach to prepare multi-material objects by DLP 3D printing by changing the resins in a single vat. The instrumentation described here can be incorporated into commercial printers. To exemplify the potential of this approach, we demonstrate the fabrication of multi-component objects, which include fluorescent materials and conductive tracks for sensor applications. Microfluidic channels were also printed as narrow as 43 μm aiming for microchip electrophoresis applications.

2. Experimental

2.1. Reagents, materials, and instruments

Two conductive resins were developed by adding poly(3,4-ethylenedioxythiophene)–polystyrenesulfonate (PEDOT:PSS) (Sigma-Aldrich, Saint Louis, MO, USA) or 3D-ADD CuEK1 (Resyner Technologies S. L., Barcelona, Spain) to a mix of the oligomers Ebecryl 8210 and Sartomer SR494 and the photoinitiator 2,4,6 trimethylbenzoyl-diphenyl-

phosphineoxide (TPO) purchased from Allnex (Paraná, PR, Brazil). Flexible-transparent and rigid-colored resins were purchased from Siraya Tech (San Gabriel, CA, USA). The water-soluble resin was from Resyner Technologies S. L. (Barcelona, Spain). Peristaltic pumps were purchased from Robocore (São Paulo, SP, Brazil), and stepper motors model Nema 23 were from Forseti (São Paulo, SP, Brazil). Plastic tubes, tube and nipple connections, and adaptors were purchased from local vendors.

The viscosity of the resins was measured with a model NDJ-8S rotational viscometer (Goyojo Instruments, Hangzhou, China).

2.2. 3D printing platform

The next subsections describe the protocols to reproduce the printing platform used throughout this work. The structure of the instrument is based on a Bene5 mono msla kit from Nova3D (Shenzhen Nova Intelligent Technology, Guangdong, Shenzhen, China). Assembly of resin vat, peristaltic pumps, resin reservoirs, vat inclination system, Z-motor, and ultraviolet illumination system is addressed in detail, including open source solutions for hardware and firmware. Although a completely new printer was developed in this work, the information depicted here can also be used to perform simple adaptations of commercial printers. Fig. 1 shows the main parts of the developed printer.

2.2.1. Light source, hardware, and software. We used a ZS Electro model PDC07-30 as a projector (Xiamen, China) based on a digital micromirror device (DMD) model DLP1438ZE (Texas Instruments, TX, USA). This illumination system works with a fixed focal distance of 25 mm and 3840 × 2160 resolution, projecting pixels with a size of 35 μm at a wavelength of 405 nm (ESI† Table S1). The projector was positioned inside the case of the printer at the front/top/left corner (see ESI,† Fig. S1a), mostly because in our prototype, we had enough space at this position, but the projector can be placed in an available space given the correct positioning of the mirrors for projection in the resin vat. Obviously, in commercial printers, the DLP projector is already mounted, or the light source and liquid crystal display in LCD 3D printers. Details of the projector can be found in the ESI† (Fig. S1).

The projector module is equipped with HDMI and DisplayPort connectors for video input, a USB connector, and I^2C ports for digital control. The control of the status and light intensity was made through the board NanoDLP v1.4 (Hangzhou, China) and managed by using a microcontroller Raspberry Pi® running with the drive TMC2226 (Ncam Multitech, Goiânia, GO, Brazil). The NanoDLP board is used with open-source software under GNU Public License (GPL) v2.0 and configured with RepRap open-source firmware, available for download in the ESI.† The Raspberry Pi® executes the front-end NanoDLP and the control software (downloaded from **https://www.nano3dtech.com/nanodlp-features/**). The software allows the setting of the printing parameters and offers a slicer and web interface that can be accessed remotely. The software communicates with the NanoDLP board through the open-source firmware Marlin (under GPL v3.0 license) for the *z*-axis control.

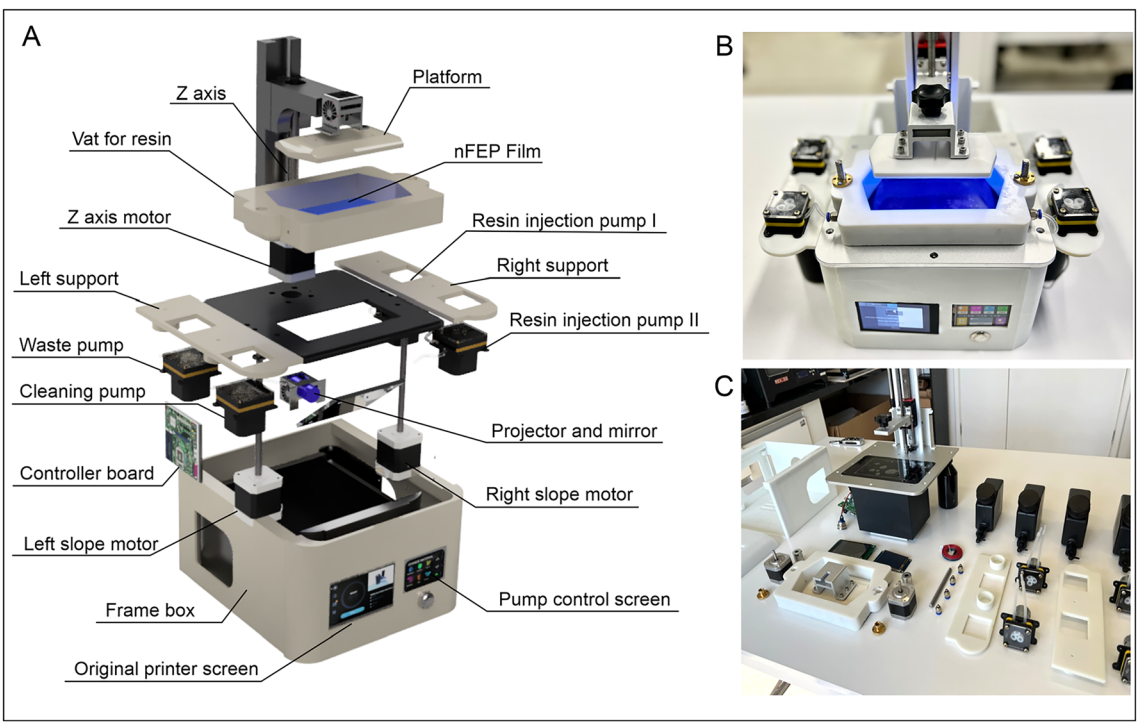

Fig. 1 (A) Exploded view with the main parts, (B) assembled and (C) unassembled developed printer.

2.2.2. Resin vat and inclination system. The inclination vat system developed in this work plays a key role in the multi-material fabrication. The firmware Marlin was configured to control two stepper motors. The motor shafts were tied to endless thread bars aligned with two holes in the resin vat (see Fig. S2 in ESI†). By actuating the motors, the vat is tilted in order to drain the resin. TCST2103 optical end-stop switches were used to limit and reproduce the tilt angle of 30°.

The vat, as well as the printing platform, was made in castable resin (Cerâmica, Melting 3D, Louveira, SP, Brazil) using a commercial Anycubic M3 MAX DLP printer. After printing, the part was post-processed at 200 °C to improve the mechanical resistance, material compatibility, and ease of cleaning. The design of the vat includes lateral channels to allow the filling of the vat with different resins and cleaning solvents. In our printer prototype, as a proof of concept, we included two peristaltic pumps to inject different resins into the vat. This way, it is possible to inject two resins automatically. For more than two different materials, the resin reservoir must be manually replaced. Although this seems a limitation, additional reservoirs and channels may be designed to accommodate the automatic replacement of more materials.

Quick fittings were used to connect 2 mm i.d. polypropylene tubes (Fig. S3 and S4 in ESI†). Flexible couplers to connect the stepper motor and vat screw nuts axes were also included in the design. This avoided

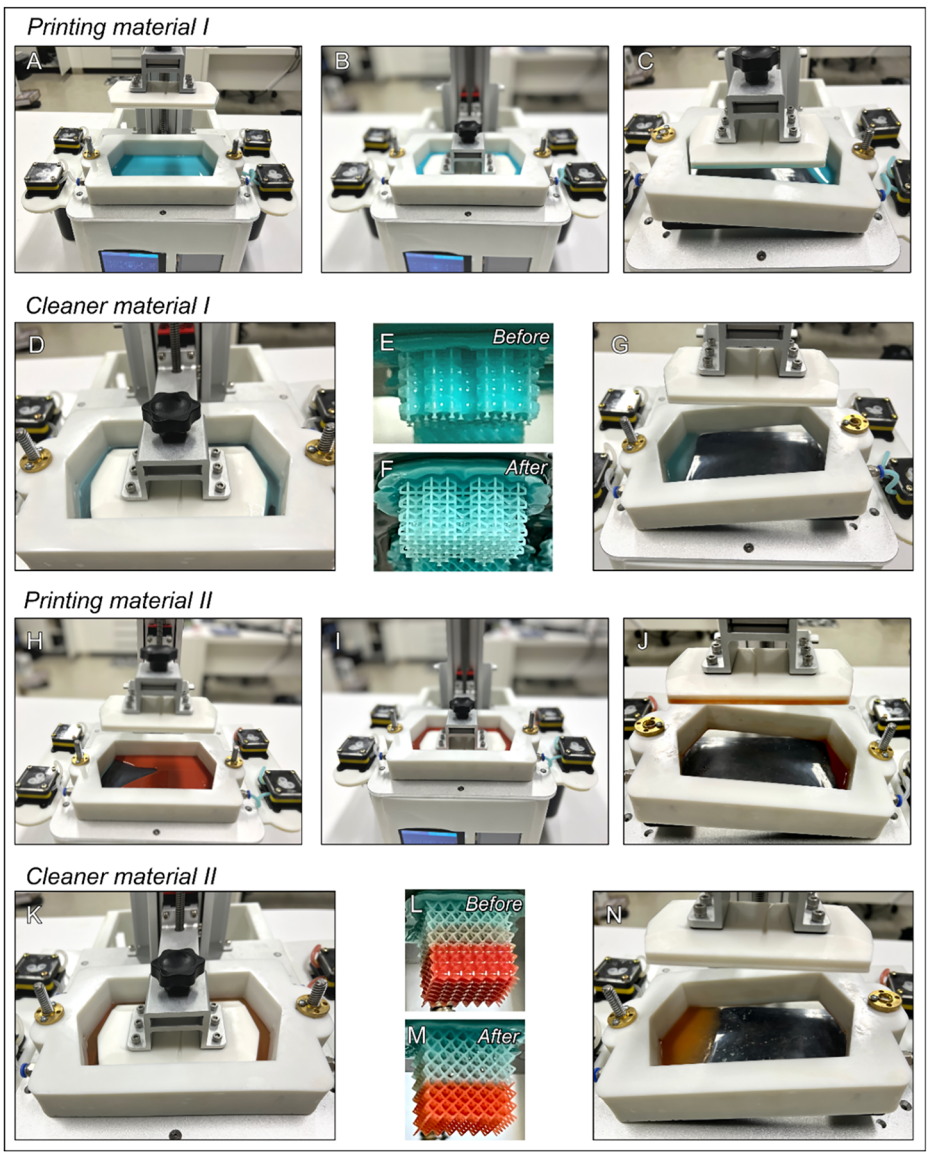

Fig. 2 Multi-material 3D printing protocol. First, the material is injected (A), polymerized (B), and removed (C). After the vat is cleaned (D) and the residues are drained (G). The second material is injected (H), polymerized (I), and removed (J), and the vat is cleaned again (K) and (N). The process can be repeated many times as needed to build complex multi-material objects. Insets show the appearance of the parts before (E and L) and after (F and M) the cleaning step.

unnecessary tension in these parts during the inclination of the vat. The design and final assembled part can be seen in Fig. S4.† Designs of vats that fit in some commercial printers are also available in ESI.†

A system of accommodation of the fluorinated ethylene propylene (FEP) (Anycubic FEP Photon Mono X-1200 × 280 cm, Quanton3D, Brazil) film was included in the vat to improve the printing performance. The film was cut into the desired dimensions and held in place in the bottom of the vat through 14 screws (see ESI† S4). The FEP film is a consumable part and must be substituted periodically to assure a good printing quality, but it usually lasts several months. The vat sat directly over the glass window on the Bene5 mono msla structure.

The build plate, where the printed part adhered during the printing, was also designed to allow easy cleaning and material exchange. The design in angle (Fig. S5 in ESI†) allows the use of up to 50 mL of resin without soiling the plate support, which facilitates the cleaning between material switching. The STL file of the built plate is available for download in the ESI.†

3. Results and discussion

3.1. Principles of operation

The proposed multi-material 3D printing system is based on the replacement of resins in a single vat, which was designed to optimize the resin exchange without cross-contamination and resin loss. Although a complete printer was built, the procedure described here can be adapted for commercial DLP or LCD 3D printers.

The printing protocol is depicted in Fig. 2 and is based on the following steps: (1) the first material is injected into the vat by using a peristaltic pump; (2) the layers are formed by exposure of the material 1 (as normally is done in single material printers); (3) the built plate is elevated, the vat is tilted to the right and the same peristaltic pump is used to aspirate the resin to the respective reservoir; (4) the vat is placed on the normal position, and a cleaning solvent is injected by a second peristaltic pump (we used ethanol in all our printings); a third peristaltic pump is used to drain the solvent residues; (5) after cleaning, the vat is set to the normal position and the second material is injected by using a fourth peristaltic pump. The vat washing procedure also allows the cleaning of the previously printed layers since the volume of solvent injected is enough to partially cover the building platform. Steps 1 to 5 are repeated until the whole object is printed. Also, more than two different materials can be combined just by changing the resin reservoirs. The whole protocol can be automated since the commands to actuate the inclination system and turn on–off the pumps can be added to the G code. Alternatively, the pumps and the stepper motors for the inclination of the vat can be independently accessed by pausing the printing. Having this option in mind, an additional control board and a panel were installed for manual operation. Examples of the G code generation for multi-material printing can be found in Fig. S6 and S7 in the ESI.† In this case, the printer must be used with slicer software and G code editing in a more intuitive way, in which we use the NanoDLP open source software. An example of the commands used is available in Fig. S6 in ESI.† Both software and all printer general control files are available from the ESI† and can be used under GNU General Public License v2.0. A video file exemplifying the whole process is also available for download in the ESI.†

We studied the flow time as a function of the inclination angle, according to the viscosity of the resins used in this work (Table S2 in the ESI†), to get a suitable time for resin removal with a minimum of residues left in the vat. We found that by using 5 mL of resin, an angle of 30°, and a flow time of 60 s, it was possible to recover 95% of the material in the vat (see Fig. S3 and S4 in ESI†). High-viscosity resins (>500 cps at 25 °C) favor the 3D printing of microfluidic channels and objects of complex geometries without the need of supports. However, vat filling and removal take longer and printing failure can occur due to incomplete filling between layers. Conversely, the use of low-viscosity resins (<300 cps at 25 °C) helps in filling the orifices between layers and makes the vat cleaning easier, but the printing parts tend to be more fragile.[62,63]

3.2. Application examples

The combination of different materials is mandatory in the field of sensor development. In most sensors, including point-of-care devices (POC) and lab-on-a-chip (microchip), it is common to find hydrophobic and hydrophilic, porous and non-porous, rigid and flexible, conductive and insulator, opaque and transparent, among other materials, which can be combined to construct complete devices suitable to perform complex tasks and analyses. Multi-material 3D printing has great potential to fill the gap in sensor development. The next examples make clear that this technique is a powerful tool on microfabrication too.

In Fig. 3A and B, a stylized yin-yang rod is illuminated by daylight (3A) and under 405 nm illumination. The rod was printed in clear resin GEM 1 (see Table S2 in ESI,† and the same GEM 1 resin modified with the blue fluorescent pigment XUK473/3019 supplied by Hycote (**https://www.hycote.co.uk/wp-content/uploads/Fluorescent-Paints-v05-2013.pdf**). Fig. 3C–E shows a two-component card also prepared in clear resin GEM 1 developed in this work and modified with fluorophores in resin powder pigment, TE3XWUJJJ, purchased from Corion (**https://www.corionshop.com.br/po-glow**). The device was illuminated by daylight (3C), 405 nm (3D), and daylight after UV exposure (3E) where it is possible to see the phosphorescence of the dye. Fig. 4A depicts a multi-material dice printed in flexible (Siraya Tech, Tenacious Flexible), rigid-clear (Siraya Tech, Blu-Tough Resin), and water-soluble (3Dresyn, IM-HT-WS) resins. In Fig. 4B, four concentric cubes were printed using (Siraya Tech, Tough

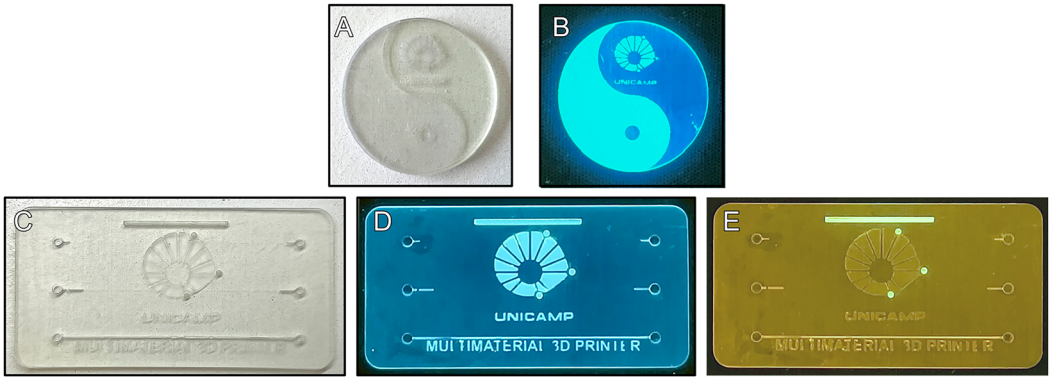

Fig. 3 Example of two-component multi-material 3D printing. Stylized yin-yang rod illuminated under daylight (A) and 405 nm (B). The rod was printed in clear GEM 1 resin and the same resin containing a fluorescent pigment. Card printed in clear GEM 1 resin and the same resin containing phosphorescent pigment visualized under daylight (C), 405 nm (D), and daylight after UV exposure (E). Composition of the resins can be found in the ESI† Table S2.

Resin) resin containing dyes (3DLab, kit Pigments for 3D resins).

Conductive parts and tracks are essential to build complete and autonomous sensor devices. Conductive materials play a central role in the development of electrochemical and physical sensors, actuation systems, electrodes for flow control (electroosmotic pumping) and electrophoretic separation, electromagnetic shielding, and embedded electronics. We have prepared two conductive-photopolymerizable resins based on PEDOT:PSS and copper nanoparticles (CuNP) dispersed in clear resin GEM 1. The electrical data of these conductive resins were evaluated in 300 μm thickness layers of the conductive material. We obtained resistivity of 35 and 85 Ω m and conductivity of 0.7 and 0.5 S m^{-1} for PEDOT:PSS and CuNP-based resins, respectively. Although we expect to develop applications in sensing using these conductive materials, here, we demonstrate as a proof-of-concept of the potential use of multi-material 3D printing on the construction of a printed circuit board containing tracks made in both PEDOT and CuNP (Fig. 5A) and flexible conductive tracks used to turn on a light emitting diode (Fig. 5B). Based on these examples, the potentiality of the printing system for applications involving wearable devices is clear.

As the ultimate goal of this work, we demonstrate the application of this high-resolution and affordable 3D printer in the fabrication of microfluidic channels. Fig. 6 depicts two microfluidic systems with typical cross-shaped channels to perform capillary microchip electrophoresis coupled with a pair of electrodes for contactless conductivity detection[16] (Fig. 6A and C). Additionally, a single-straight channel surrounded by a spiral channel (Fig. 6B and D) was 3D printed. Optical microscopy was used to measure the cross-section of the printed microchannels, obtaining values of 43 μm (Fig. 6E).

Compared to previously reported works in the literature, our approach does not require changing the resin vat, allows large printing volume with a pixel size of 35 μm, with minimal waste of resin. Moreover, the vat inclination system can be implemented in commercial DLP printers and the ESI† (S8 and S9) lists the necessary components for the modification of two selected commercial printers (Nova3D Bene6 and Anycubic DLP D2). Our approach is also prone to fully automation, to allow the required number of materials to be printed. The iCLIP approach proposed by Lipkowitz *et al.*[59] is also versatile in producing multi-material with accelerated printing speeds, but requires the use of viaducts in the design of the objects, which can make the production of microfluidic devices more difficult. This drawback is not

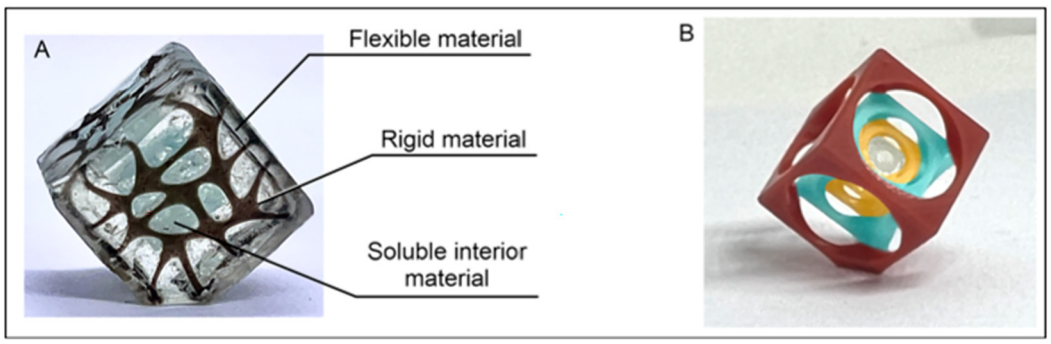

Fig. 4 Examples of complex multi-material objects. (A) Dice formed in flexible, rigid-clear, and water-soluble resins. (B) Concentric cubes prepared in clear resin containing dyes.

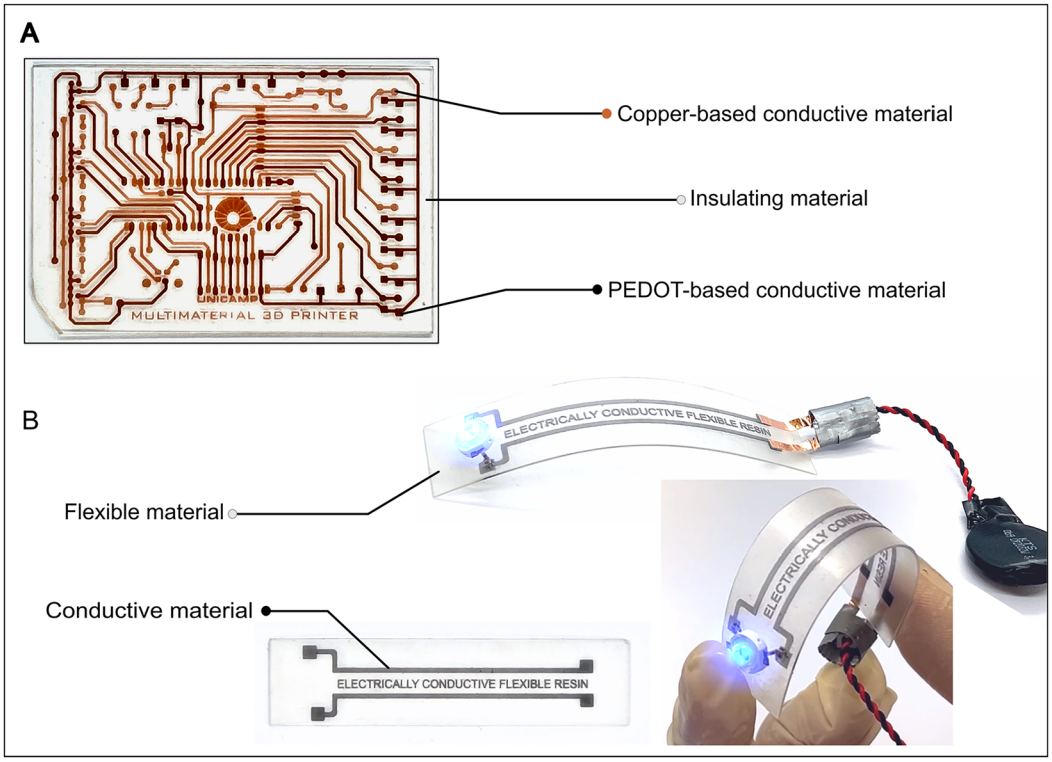

Fig. 5 Example of multi-material printed devices containing conductive parts. (A) A printed circuit board was built in flexible resin (insulator) and PEDOT-based and CuNP-based conductive resins. (B) A flexible device was printed in GEM 1 resin and PEDOT-based conductive tracks. It was possible to supply a light-emitting diode, even after bending the device.

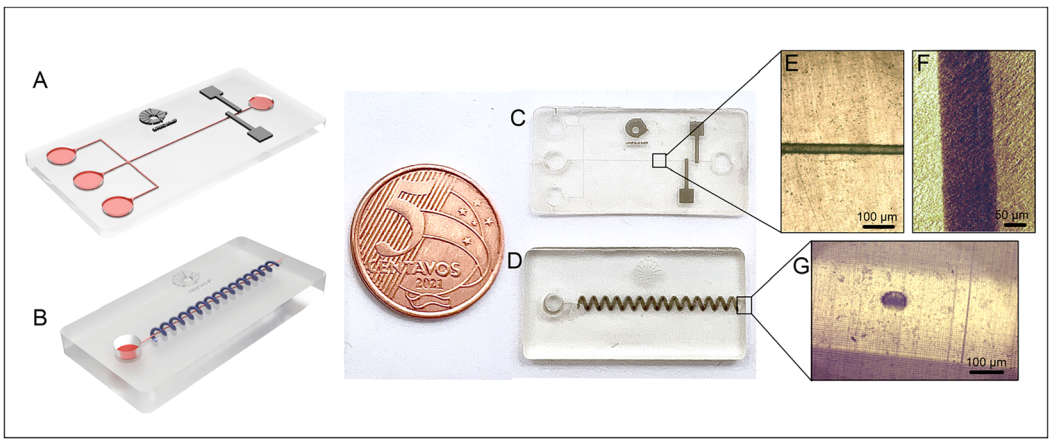

Fig. 6 Microfluidic multi-material devices. (A and C) Capillary microchip electrophoresis containing conductive electrodes to perform contactless conductivity detection. (B and D) Straight channel surrounded by a spiral microchannel. (E) Optical microscopy of the cross-section of microfluidic channels. (F) Cross-section of deposition of 5 layers (10 μm each) of conductive resin (electrode) between layers of insulating material. (G) Cross-section of the microfluidic channel.

found in our proposed peristaltic pumping and vat inclination systems for resin replacement and vat cleaning.

4. Conclusion

With the reduction in costs of both printers and supplies, the use of 3D printing techniques is becoming attractive for microfluidic device prototyping.

Multi-material 3D printing holds enormous potential for producing microfluidic devices in an unprecedented way. We described a simple procedure to produce objects containing combined materials in order to prepare complex objects and functional microfluidic devices. Although we have built the whole system, the modification can be incorporated into commercially available printers. By using a high resolution projector, we were able to produce

microfluidic devices containing channels as narrow as 43 μm.

By adding fluorescent or phosphorescent molecules to the resin formulation, it is possible to design and 3D print optical sensors. The incorporation of conductive tracks to the microfluidic devices opens a wide range of possibilities to integrate electrochemical sensors, as well as electrodes for application of electric field for electrophoresis, dielectrophoresis, cell manipulation, and sorting.

Author contributions

Reverson F. Quero: conceptualization, data curation, methodology, investigation, validation, software, resources, writing – review & editing. Dosil P. de Jesus: resources, funding acquisition, writing – review & editing. José Alberto F. da Silva: conceptualization, resources, investigation, funding acquisition, project administration, writing – original draft/review & editing.

Conflicts of interest

The authors declare no conflict of interest.

Acknowledgements

The authors acknowledge the financial support provided by Fundação de Amparo à Pesquisa do Estado de São Paulo (FAPESP grants #2013/22127-2, #2018/13496-8, 2018/06478-3), National Council for Scientific and Technological Development (CNPq grant #140545/2017-4, #305447/2019-0), Instituto Nacional de Ciência e Tecnologia em Bioanalítica (INCTBio grant #2014/50867-3 FAPESP), and Coordenação de Aperfeiçoamento de Pessoal do Ensino Superior (CAPES, #88887.372944/2019-00 – Finance code 001).

References

1 Y.-J. Juang and Y.-J. Chiu, Fabrication of Polymer Microfluidics: An Overview, *Polymers*, 2022, **14**, 2028.
2 A. Manz, N. Graber and H. M. Widmer, Miniaturized Total Chemical Analysis Systems: a Novel Concept for Chemical Sensing, *Sens. Actuators, B*, 1990, **1**, 244–248.
3 C. T. Culbertson, *et al.*, Micro Total Analysis Systems: Fundamental Advances and Biological Applications, *Anal. Chem.*, 2014, **86**, 95–118.
4 D. C. Duffy, *et al.*, Rapid Prototyping of Microfluidic Systems in Poly(dimethylsiloxane), *Anal. Chem.*, 1998, **70**, 4974–4984.
5 T. Nguyen, *et al.*, Multilayer Soft Photolithography Fabrication of Microfluidic Devices Using a Custom-Built Wafer-Scale PDMS Slab Aligner and Cost-Efficient Equipment, *Micromachines*, 2022, **13**, 1357.
6 G. I. J. Salentijn, *et al.*, Fused Deposition Modeling 3D Printing for (Bio)analytical Device Fabrication: Procedures, Materials, and Applications, *Anal. Chem.*, 2017, **89**, 7053–7061.
7 P. E. Oomen, *et al.*, Controlled, synchronized actuation of microdroplets by gravity in a superhydrophobic, 3D-printed device, *Anal. Chim. Acta*, 2017, **988**, 50–57.
8 A. I. Shallan, *et al.*, Cost-Effective Three-Dimensional Printing of Visibly Transparent Microchips within Minutes, *Anal. Chem.*, 2014, **86**, 3124–3130.
9 J. L. Erkal, *et al.*, 3D printed microfluidic devices with integrated versatile and reusable electrodes, *Lab Chip*, 2014, **14**, 2023–2032.
10 K. B. Anderson, *et al.*, A 3D Printed Fluidic Device that Enables Integrated Features, *Anal. Chem.*, 2013, **85**, 5622–5626.
11 L. P. Bressan, *et al.*, Low-cost and simple FDM-based 3D-printed microfluidic device for the synthesis of metallic core-shell nanoparticles, *SN Appl. Sci.*, 2020, **2**, 984.
12 L. P. Bressan, *et al.*, A simple procedure to produce FDM-based 3D-printed microfluidic devices with an integrated PMMA optical window, *Anal. Methods*, 2019, **11**, 1014–1020.
13 L. P. Bressan, *et al.*, 3D-printed microfluidic device for the synthesis of silver and gold nanoparticles, *Microchem. J.*, 2019, **146**, 1083–1089.
14 J. E. Esene, *et al.*, 3D printed microfluidic device for automated, pressure-driven, valve-injected microchip electrophoresis of preterm birth biomarkers, *Microchim. Acta*, 2022, **189**, 204.
15 J. L. S. Noriega, *et al.*, Spatially and optically tailored 3D printing for highly miniaturized and integrated microfluidics, *Nat. Commun.*, 2021, **12**, 5509.
16 B. M. C. Costa, *et al.*, 3D-printed microchip electrophoresis device containing spiral electrodes for integrated capacitively coupled contactless conductivity detection, *Anal. Bioanal. Chem.*, 2021, **414**, 545–550.
17 M. J. Beauchamp, *et al.*, 3D Printed Microfluidic Devices for Microchip Electrophoresis of Preterm Birth Biomarkers, *Anal. Chem.*, 2019, **91**, 7418–7425.
18 H. Gong, A. T. Woolley and G. P. Nordin, 3D printed high density, reversible, chip-to-chip microfluidic interconnects, *Lab Chip*, 2018, **18**, 639–647.
19 M. J. Beauchamp, G. P. Nordin and A. T. Woolley, Moving from millifluidic to truly microfluidic sub-100-μm cross-section 3D printed devices, *Anal. Bioanal. Chem.*, 2017, **409**, 4311–4319.
20 H. Gong, *et al.*, Custom 3D printer and resin for 18 μm × 20 μm microfluidic flow channels, *Lab Chip*, 2017, **17**, 2899–2909.
21 H. Gong, A. T. Woolley and G. P. Nordin, High density 3D printed microfluidic valves, pumps, and multiplexers, *Lab Chip*, 2016, **16**, 2450–2458.
22 H. Gong, *et al.*, Optical approach to resin formulation for 3D printed microfluidics, *RSC Adv.*, 2015, **5**, 106621–106632.
23 C. I. Rogers, *et al.*, 3D printed microfluidic devices with integrated valves, *Biomicrofluidics*, 2015, **9**, 016501.
24 R. F. Quero, *et al.*, Understanding and improving FDM 3D printing to fabricate high-resolution and optically transparent microfluidic devices, *Lab Chip*, 2021, **21**, 3715–3729.

25 N. P. Macdonald, *et al.*, Comparing Microfluidic Performance of Three-Dimensional (3D) Printing Platforms, *Anal. Chem.*, 2017, **89**, 3858–3866.
26 S. Waheed, *et al.*, 3D printed microfluidic devices: enablers and barriers, *Lab Chip*, 2016, **16**, 1993–2013.
27 B. Gross, S. Y. Lockwood and D. M. Spence, Recent Advances in Analytical Chemistry by 3D Printing, *Anal. Chem.*, 2017, **89**, 57–70.
28 C. Chen, *et al.*, 3D-printed microfluidic devices: fabrication, advantages and limitations—a mini review, *Anal. Methods*, 2016, **8**, 6005–6012.
29 G. Gonzalez, *et al.*, Current and emerging trends in polymeric 3D printed microfluidic devices, *Addit. Manuf.*, 2022, **55**, 102867.
30 A. V. Nielsen, *et al.*, 3D Printed Microfluidics, *Annu. Rev. Anal. Chem.*, 2019, **13**, 1.1–1.21.
31 U. Kalsoom, P. N. Nesterenko and B. Paull, Current and future impact of 3D printing on the separation sciences, *TrAC, Trends Anal. Chem.*, 2018, **105**, 492–502.
32 F. Cecil, *et al.*, One step multi-material 3D printing for the fabrication of a photometric detector flow cell, *Anal. Chim. Acta*, 2020, **1097**, 127–134.
33 E. Fornells, *et al.*, Integrated 3D printed heaters for microfluidic applications: Ammonium analysis within environmental water, *Anal. Chim. Acta*, 2020, **1098**, 94–101.
34 U. Kalsoom, *et al.*, Low-Cost Passive Sampling Device with Integrated Porous Membrane Produced Using Multimaterial 3D Printing, *Anal. Chem.*, 2018, **90**, 12081–12089.
35 F. Li, *et al.*, Increasing the functionalities of 3D printed microchemical devices by single material, multimaterial, and print-pause-print 3D printing, *Lab Chip*, 2019, **19**, 35–49.
36 R. F. Quero, *et al.*, Using multi-material fused deposition modeling (FDM) for one-step 3D printing of microfluidic capillary electrophoresis with integrated electrodes for capacitively coupled contactless conductivity detection, *Sens. Actuators, B*, 2022, **365**, 131959.
37 S. Akbari, *et al.*, Multimaterial 3D Printed Soft Actuators Powered by Shape Memory Alloy Wires, *Sens. Actuators, A*, 2019, **290**, 177–189.
38 V. G. Rocha, *et al.*, Direct ink writing advances in multi-material structures for a sustainable future, *J. Mater. Chem. A*, 2020, **8**, 15646–15657.
39 U. Shaukat, E. Rossegger and S. Schlögl, A Review of Multi-Material 3D Printing of Functional Materials via Vat Photopolymerization, *Polymers*, 2022, **14**, 2449.
40 S. Maruo, K. Ikuta and T. Ninagawa, Multi-polymer microstereolithography for hybrid opto-MEMS, *MEMS 2001 14th IEEE International Conference on Micro Electro Mechanical Systems*, 2001, vol. 4.
41 R. Wicker, F. Medina and C. Elkins, Multiple material micro-fabrication: extending stereolithography to tissue engineering and other novel applications, *International Solid Freeform Fabrication Symposium*, 2004, vol. 11.
42 A. Inamdar, *et al.*, Development of an automated multiple material stereolithography machine, *Proceedings of the SFF Symposium Proceedings*, 2006, vol. 12.
43 J.-W. Choi, E. MacDonald and R. Wicker, Multi-material microstereolithography, *Int. J. Adv. Manuf. Technol.*, 2010, **49**, 543–551.
44 K. Arcaute, B. Mann and R. Wicker, Stereolithography of spatially controlled multi-material bioactive poly(ethylene glycol) scaffolds, *Acta Biomater.*, 2010, **6**, 1047–1054.
45 J.-W. Choi, H.-C. Kim and R. Wicker, Multi-material stereolithography, *J. Mater. Process. Technol.*, 2011, **211**, 318–328.
46 R. B. Wicker and E. W. MacDonald, Multi-material, multi-technology stereolithography, *Virtual Phys. Prototyp.*, 2012, **7**, 181–194.
47 A. Joe Lopes, E. MacDonald and R. B. Wicker, Integrating stereolithography and direct print technologies for 3D structural electronics fabrication, *Rapid Prototyp. J.*, 2012, **18**, 129–143.
48 D. Espalin, *et al.*, 3D Printing multifunctionality: structures with electronics, *Int. J. Adv. Manuf. Technol.*, 2014, **72**, 963–978.
49 Q. Ge, *et al.*, Multimaterial 4D Printing with Tailorable Shape Memory Polymers, *Sci. Rep.*, 2016, **6**, 31110.
50 Q. Wang, *et al.*, Lightweight Mechanical Metamaterials with Tunable Negative Thermal Expansion, *Phys. Rev. Lett.*, 2016, **117**, 175901.
51 K. Kowsari, *et al.*, High-Efficiency High-Resolution Multimaterial Fabrication for Digital Light Processing-Based Three-Dimensional Printing. 3D Print, *Addit. Manuf.*, 2018, **5**, 185–193.
52 K. Kowsari, *et al.*, Photopolymer formulation to minimize feature size, surface roughness, and stair-stepping in digital light processing-based three-dimensional printing, *Addit. Manuf.*, 2018, **24**, 627–638.
53 B. Zhang, *et al.*, Highly stretchable hydrogels for UV curing based high-resolution multimaterial 3D printing, *J. Mater. Chem. B*, 2018, **6**, 3246–3253.
54 Y. F. Zhang, *et al.*, Miniature Pneumatic Actuators for Soft Robots by High-Resolution Multimaterial 3D Printing, *Adv. Mater. Technol.*, 2019, **4**, 1900427.
55 Y. Kim, *et al.*, Digital Manufacturing of Selective Porous Barriers in Microchannels Using Multi-Material Stereolithography, *Micromachines*, 2018, **9**, 125.
56 B. Khatri, *et al.*, Development of a multi-material stereolithography 3D printing device, *Micromachines*, 2020, **11**, 532.
57 H. Mao, *et al.*, Multi-material stereolithography using curing-on-demand printheads, *Rapid Prototyp. J.*, 2021, **27**, 861–871.
58 I. Ahmed, K. Sullivan and A. Priye, Multi-Resin Masked Stereolithography (MSLA) 3D Printing for Rapid and Inexpensive Prototyping of Microfluidic Chips with Integrated Functional Components, *Biosensors*, 2022, **12**, 652.

59 G. Lipkowitz, *et al.*, Injection continuous liquid interface production of 3D objects, *Sci. Adv.*, 2022, **8**, eabq3917.
60 F. Mayer, *et al.*, Multimaterial 3D laser microprinting using an integrated microfluidic system, *Sci. Adv.*, 2019, **5**, eaau9160.
61 A. C. Lamont, *et al.*, A facile multi-material direct laser writing strategy, *Lab Chip*, 2019, **19**, 2340–2345.
62 S. Y. Song, *et al.*, Optimization and characterization of high-viscosity ZrO2 ceramic nanocomposite resins for supportless stereolithography, *Mater. Des.*, 2019, **180**, 107960.
63 T. Zandrini, *et al.*, Effect of the resin viscosity on the writing properties of two-photon polymerization, *Opt. Mater. Express*, 2019, **9**, 2601–2616.